# The effect of widespread early aerobic marine ecosystems on methane cycling and the Great Oxidation

Stuart J. Daines & Timothy M. Lenton*

Earth System Science group, College of Life and Environmental Sciences, University of Exeter, UK

*Corresponding author: t.m.lenton@exeter.ac.uk

## Abstract

The balance of evidence suggests that oxygenic photosynthesis had evolved by 3.0–2.7 Ga, several hundred million years prior to the Great Oxidation ≈2.4 Ga. Previous work has shown that if oxygenic photosynthesis spread globally prior to the Great Oxidation, this could have supported widespread aerobic ecosystems in the surface ocean, without oxidizing the atmosphere. Here we use a suite of models to explore the implications for carbon cycling and the Great Oxidation. We find that recycling of oxygen and carbon within early aerobic marine ecosystems would have restricted the balanced fluxes of methane and oxygen escaping from the ocean, lowering the atmospheric concentration of methane in the Great Oxidation transition and its aftermath. This in turn would have minimised any bi-stability of atmospheric oxygen, by weakening a stabilising feedback on oxygen from hydrogen escape to space. The result would have been a more reversible and probably episodic rise of oxygen at the Great Oxidation transition, consistent with existing geochemical evidence. The resulting drop in methane levels to ≈10 ppm is consistent with climate cooling at the time but adds to the puzzle of what kept the rest of the Proterozoic warm. A key test of the scenario of abundant methanotrophy in oxygen oases before the Great Oxidation is its predicted effects on the organic carbon isotope ($\delta^{13}C_{org}$) record. Our open ocean general circulation model predicts $\delta^{13}C_{org}$ ≈ -30 to -45 ‰ consistent with most data from 2.65–2.45 Ga. However, values of $\delta^{13}C_{org}$ ≈ -50 ‰ require an extreme scenario such as concentrated methanotroph production where shelf-slope upwelling of methane-rich water met oxic shelf water.

**Keywords**

Great Oxidation; modelling; methane; oxygen; methanotrophy; carbon isotope record

## 1. Introduction

Multiple lines of evidence suggest that oxygenic photosynthesis evolved long before the oxygenation of the atmosphere (Farquhar et al., 2011), and spread to oxygenate regions of the surface environment in the late Archean (Buick, 1992; Czaja et al., 2012; Eigenbrode and Freeman, 2006; Kasting, 1991; Kendall et al., 2010; Lalonde and Konhauser, 2015; Olson et al., 2013; Riding et al., 2014). There is evidence for oxidative weathering on the continents, perhaps as early as 3.0-2.9 Ga from chromium (Crowe et al., 2013) and molybdenum (Planavsky et al., 2014) isotope fractionation. By 2.7-2.5 Ga, rising sedimentary concentrations of Mo and Re and Mo isotope fractionation indicate oxidative weathering (Siebert et al., 2005; Wille et al., 2007), trends in sulphur isotopes suggest localised oxygen production (Zerkle et al., 2012), and by 2.5 Ga sulphide accumulation in the ocean suggests more intense oxidative weathering (Reinhard et al., 2009). In the oceans, rare earth element analyses reveal a shallow shelf sea oxygen oasis 2.8 Ga (Riding et al., 2014). Coupled iron and molybdenum isotope fractionation provides evidence of surface ocean oxygen oases 2.68-2.5 Ga (Czaja et al., 2012), and changes in the abundance of Mo and Re with sediment depth 2.6–2.5 Ga indicate dissolved $O_2$ at shallow depth along ocean margins (Kendall et al., 2010). Consistent with the appearance of oxygen, protein fold evolution (Wang et al., 2011) and gene phylogeny (David and Alm, 2011) both show a rapid burst of evolutionary innovation including aerobic metabolisms in the Late Archean >2.5 Ga and possibly >2.85 Ga (David and Alm, 2011). Others have postulated a late origin of oxygenic photosynthesis ≈2.4 Ga leading immediately to the Great Oxidation (Kopp et al., 2005), but we find the geochemical evidence for oxygen production compelling by at latest ≈2.7 Ga, and we take this as our working hypothesis in trying to explain the geochemical record.

The observed Mass Independent Fraction of Sulphur isotopes (MIF of S) until at least 2.45 Ga (Farquhar et al., 2011), indicates a very low atmospheric $pO_2 < 10^{-5}$ PAL (Present Atmospheric Level), and a high atmospheric concentration of methane (Zahnle et al., 2006). This can be reconciled with abundant evidence for oxygen production, at least from an atmospheric point of view. Previous modelling work has shown that the key overall determinant of atmospheric redox state in the Late Archean would have been the net overall oxidant/reductant balance of fluxes to and from the surface Earth system, including hydrogen escape to space, organic carbon burial, and exchange with the crust and mantle (Claire et al., 2006; Goldblatt et al., 2006). Provided this net flux was sufficiently reducing, a low atmospheric $pO_2 < 10^{-5}$ PAL would have been maintained even in the presence of a productive oxygenic ecosystem (Goldblatt et al., 2006; Zahnle et al., 2006), because the balanced atmospheric oxygen and methane fluxes escaping from the biosphere would have been rapidly consumed by atmospheric photochemistry.

What is not fully understood is how surface ecosystems operated in the Late Archean prior to the Great Oxidation (GOE) 2.45–2.32 Ga, in particular how the geochemical evidence for a strongly reducing atmosphere and an oxygenated surface environment can be reconciled. This requires either oxidative weathering at low atmospheric oxygen levels $pO_2 < 10^{-5}$ PAL, transient 'whiffs' of oxygen as yet unresolved in the sulphur MIF record, or localized oxygen production and consumption. Microbial mats represent an environment where the production and consumption of oxygen and organic carbon were very closely coupled, potentially reconciling the occurrence of oxidative weathering on land with a very reducing atmosphere (Herman and Kump, 2005; Lalonde and Konhauser, 2015). In the ocean, following the evolution of planktonic oxygenic photosynthesis, a partially oxygenated surface ocean could have coexisted with a reducing atmosphere and an anoxic deep ocean, in a state of disequilibrium maintained by high rates of oxygen production in the water and relatively slow air-sea gas exchange (Kasting, 1991; Olson et al., 2013).

Multiple biogeochemical pathways potentially could have contributed directly or indirectly to oxygen cycling within early ecosystems. Aerobic respiration of organic carbon may have been ubiquitous (Towe, 1990), especially if aerobic respiration is a more ancient metabolism than oxygenic photosynthesis. This has received some recent support from measurements of aerobic growth occurring at nanomolar $O_2$ concentrations (Stolper et al., 2010), where modelling has indicated that such concentrations could have been reached even via abiotic mechanisms prior to the origin of oxygenic photosynthesis (Haqq-Misra et al., 2011). A fraction of the organic carbon fixed by oxygenic photosynthesis would have been converted to methane by fermentation and methanogenesis, and then potentially consumed by aerobic methanotrophs, giving a mechanism to explain isotopically very light Late Archean kerogens (Hayes, 1983; Hayes, 1994). In the Hamersley Province, Western Australia, where evidence for oxygenic photosynthesis is compelling (Buick, 1992), these kerogens have minimum $\delta^{13}C_{org}$ ≈ -60‰ from shallower water sediments 2.72 Ga, and minimum $\delta^{13}C_{org}$ ≈-50 ‰ from deeper water sediments 2.65–2.6 Ga, weakening to a minimum $\delta^{13}C_{org}$ ≈ -35 ‰ by 2.45 Ga (Czaja et al., 2012; Eigenbrode and Freeman, 2006; Thomazo et al., 2009). Similar but less extreme environment-dependent patterns in $\delta^{13}C_{org}$ are seen in the 2.96-2.82 Ga Witwatersrand Supergroup, Transvaal, South Africa (Guy et al., 2012), and in the 2.65-2.5 Ga Ghaap Group (Zerkle et al., 2012). Any build-up of sulphate in the Late Archean ocean (Reinhard et al., 2009) could potentially have supported anaerobic oxidation of methane (AOM), but recent work suggests low sulphate concentrations ~10 μM (Crowe et al., 2014; Zhelezinskaia et al., 2014).

Previous models of Earth's long-term redox evolution in the Archean-Proterozoic (Catling et al., 2007; Claire et al., 2006; Goldblatt et al., 2006), have not resolved such aerobic ecosystems and have made different assumptions regarding methane cycling and atmospheric methane and oxygen fluxes. These models agree that the eventual rise of atmospheric oxygen in the Great Oxidation (GOE) 2.45–2.32 Ga, can be understood as being triggered by the overall balance of fluxes to and from the ocean-atmosphere (including hydrogen escape) shifting to net oxidising, for which there

97 are several candidate causes (Kasting, 2013). They also agree that once a modest redox imbalance
98 produced enough oxygen for the ozone layer to begin to form, the resulting slowing in the
99 photochemical consumption of oxygen via reaction with methane would have produced a strong
100 positive feedback, driving an abrupt oxygen rise (Claire et al., 2006; Goldblatt et al., 2006). Where
101 existing models disagree is over the nature of the GOE transition. The apparently irreversible loss of
102 the MIF of S signal, which has not reappeared since 2.32 Ga, could be explained by a bi-stability of
103 atmospheric oxygen, in which for a range of values of the overall redox balance of the surface Earth,
104 both low and high oxygen states are stable (Goldblatt et al., 2006). However, this model assumes a
105 spatial and temporal decoupling within the ocean such that marine net primary production was
106 almost entirely converted into large balanced fluxes of oxygen and methane into the atmosphere
107 prior to the Great Oxidation. An alternative model (Claire et al., 2006) assumes lower atmospheric
108 methane/oxygen fluxes and generates an abrupt but reversible GOE transition. The size of the
109 balanced methane/oxygen flux also controls the atmospheric concentration of the minority gas
110 (oxygen prior to the Great Oxidation, methane afterwards), hence it determines the methane
111 contribution to the Proterozoic greenhouse (Pavlov et al., 2003), and it may have influenced the
112 Archean sulphur MIF signature (Zerkle et al., 2012).

113 Here we seek to understand the controls on oxygen and methane cycling in Late Archean marine
114 ecosystems, and the implications for the nature of the GOE and for interpreting the carbon isotope
115 record. We take as a working hypothesis that planktonic oxygenic photosynthesis and therefore
116 oxygen oases were present in the Late Archean surface ocean. First we use an ocean general
117 circulation model and a multi-box ocean model to explore the potential for oxygen build-up in the
118 surface ocean. Then we simulate the effects of including aerobic methanotrophy in the surface
119 ocean on oxygen and methane concentrations and their balanced fluxes escaping to the
120 atmosphere. Next we used an existing model of the atmospheric redox balance (Goldblatt et al.,
121 2006) to examine the implications of the predicted oxygen/methane balanced fluxes for the nature
122 of the Great Oxidation transition. We exclude climate feedbacks (Claire et al., 2006) in the interests

of first clarifying our understanding of the key biological and chemical controls on oxygen and methane through the Great Oxidation transition. Finally, we return to the ocean models to test the hypothesis that aerobic methanotrophy was responsible for isotopically very light Late Archean kerogens (Hayes, 1983; Hayes, 1994). This leads into a discussion of the potential for spatial concentration of aerobic methanotrophy in shelf/slope upwelling regions and/or microbial mats, the effects of additional redox shuttles (such as via sulphate), and the overall implications of our results for controls on oxygen and methane concentrations before and after the Great Oxidation.

## 2. Materials and Methods

Figure 1 shows a schematic of the key processes considered in our modelling. We use a hierarchy of models to cover the wide range of space and timescales. To account for the spatially and seasonally-variable effects of potentially widespread early aerobic ecosystems, we extended the representation of biogeochemistry in the MITgcm ocean general circulation model to include methane cycling. We used the results of the GCM to inform the construction of a spatially-resolved box model utilising the same biogeochemical scheme. Then we used this ocean box model together with an existing model of the atmospheric redox balance (Goldblatt et al., 2006) to examine the effect of the predicted balanced fluxes of methane and oxygen on the Great Oxidation transition. More complete details of the models are given in the Supplementary Material. Here we concentrate on the key biogeochemical processes that govern the results.

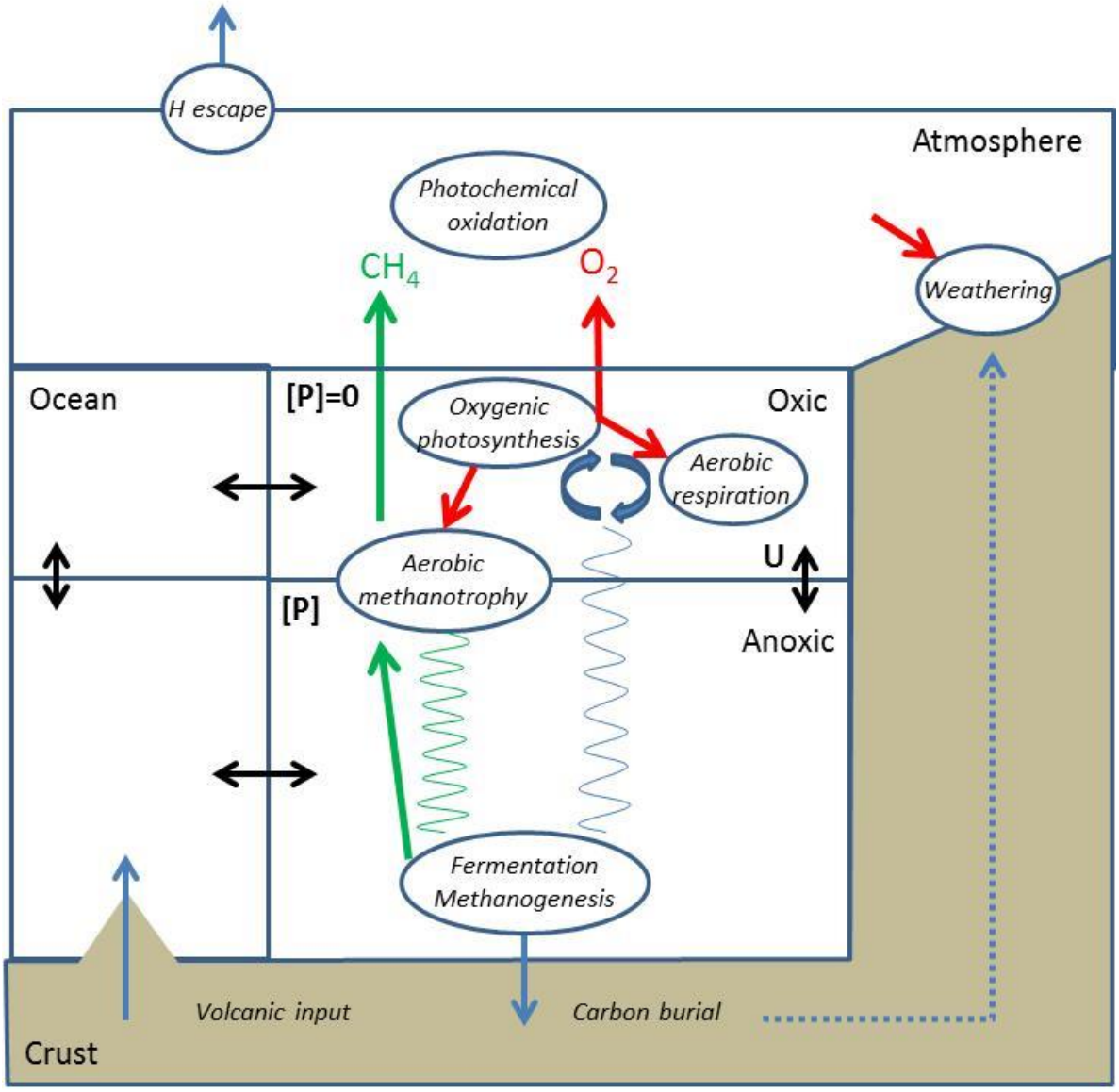


142

143 **Figure 1. Key processes in the Late Archean-Paleoproterozoic Earth system. [P] is the concentration of limiting nutrient**
144 **in the deep ocean, which is mixed upwards at rate U to the surface ocean, fuelling oxygenic photosynthesis. Some of the**
145 **oxygen liberated is consumed by aerobic respiration, recycling nutrient and boosting net primary production. The**
146 **upwelling nutrient flux determines the sinking export flux of carbon (blue wiggle). In the deep ocean this is converted by**
147 **fermentation and methanogenesis to methane (and $CO_2$). Methane upwells to the surface waters where it is partially**
148 **consumed with oxygen by aerobic methanotrophy resulting in an additional isotopically light sinking flux (green wiggle).**
149 **The remaining balanced fluxes of methane and oxygen escape to the atmosphere and are consumed by**
150 **photochemically-driven oxidation. Reductant input into the atmosphere from the crust and mantle, and from any time-**
151 **dependent imbalance between carbon burial and oxidative weathering, is balanced by escape to space of hydrogen**
152 **produced by methane photolysis. See Figure A1 for a more complete description.**

153 **2.1. Marine biogeochemistry**

154 Oxygenic photosynthesis limited by a single nutrient (P) is represented by

155 $$CO_2 + H_2O + xP + h\nu \rightarrow CH_2O(xP) + O_2$$

156 where x = $1/r_{c:p}$ and $r_{c:p}$ is a 'Redfield ratio' of carbon to phosphorus in marine phytoplankton
157 biomass.

158 Aerobic respiration results in a null cycle with no net oxygen production:

159 $$CH_2O(xP) + O_2 \rightarrow CO_2 + H_2O + xP.$$

160 The remaining biomass carbon *EP* (export production) is exported to anoxic deeper waters with a
161 balancing net $O_2$ release in the surface ocean. *EP* is remineralized by fermentation and
162 methanogenesis (in the absence of alternative electron acceptors in the low sulphate Late Archean
163 environment), producing isotopically light methane:

164 $$CH_2O(xP) \rightarrow 0.5CO_2 + 0.5CH_4 + xP.$$

165 Upwelling methane may then come into contact with surface $O_2$ and be consumed by aerobic
166 methanotrophy. We define a methanotroph growth efficiency $g_m$ (biomass produced divided by
167 methane consumed) such that the stoichiometry is given by the combination of biomass production
168 and energy releasing reactions:

169 $$g_m\,[CH_4 + O_2 + xP] + (1 - g_m)[\,CH_4 + 2O_2] \rightarrow g_m\,[CH_2O(xP) + H_2O] + (1 - g_m)[\,2H_2O + CO_2]$$

170 hence the overall methanotroph stoichiometry is given by:

171 $$CH_4 + (2 - g_m)O_2 + g_m\,xP \rightarrow g_m CH_2O(xP) + (2 - g_m)H_2O + (1 - g_m)CO_2$$

172 The isotopic composition of the net organic carbon flux to anoxic deep waters and to sediments is
173 then determined by the relative proportion of methanotroph and autotroph sinking biomass, hence

is dependent on the fraction of methane captured by methanotrophs and the methanotroph growth efficiency (Hayes, 1983; Hayes, 1994).

The remaining oxygen and methane then support a balanced flux escaping to the atmosphere, $f_{bal}$ = $f_{O2}$ = 2 $f_{CH4}$.

The marine biosphere reaches equilibrium on an ocean circulation timescale on the order of $10^4$ yr hence (for the GCM) we assume it is in steady-state relative to tectonic or evolutionary forcings.

**2.2. Atmospheric redox balance**

Biosphere/geosphere inputs into the atmosphere are represented by two control parameters: the balanced flux of oxygen and methane escaping the ocean, $f_{bal}$, and the oxygen-independent part of overall Earth surface reductant input $f_{surf}$ (i.e. not including the oxygen sensitivity of oxidative weathering). $f_{bal}$ is mostly consumed by atmospheric photochemical oxidation with net reaction:

$$2O_2 + CH_4 + h\nu \rightarrow CO_2 + 2H_2O$$

with a non-linear dependency of the reaction rate on atmospheric oxygen concentration due to the formation of the ozone layer (Goldblatt et al., 2006), and a fast equilibration timescale, on the order of $10^2$ yr.

The oxidation state of the atmosphere is determined by net oxidant and reductant budgets. A small fraction of export production ($f_{Cburial}$ ≈$10^{13}$ mol $O_2$ equiv $yr^{-1}$) is buried as reduced organic carbon, cycled via tectonic processes on timescales ≈$10^8$ yr contributing to metamorphic flux $f_{met}$, and then exposed and oxidised contributing to a surface oxidation flux $f_{ox}$. Volcanic input of reduced species from the mantle provides a net reductant input of $f_{mantle}$ ≈ $10^{11}$ mol $O_2$ equiv $yr^{-1}$. Hydrogen escape to space via methane photolysis occurs with net overall reaction:

$$CH_4 + CO_2 + O_2 + h\nu \rightarrow 2CO_2 + 4H\uparrow_{space},$$

This provides a net oxidant input $f_{hesc}$ (as methane and oxygen are produced in the ratio 1:2, but consumed in the ratio 1:1). This drives a slow overall oxidation of the Earth's surface.

The redox budget $f_{redox}$ of the atmosphere is then (all fluxes in mol $O_2$ equiv $yr^{-1}$):

$$f_{redox} = -f_{hesc}\,(p\mathrm{CH_4}) + f_{met}(t) + f_{mantle}(t) - f_{Cburial}(t) + f_{ox}(t, p\mathrm{O_2})$$

To separate the dynamics of atmospheric oxygen and methane from the tectonically and biologically driven inputs, we separate surface oxidation into time-dependent and oxygen-sensitive components $f_{ox}(t, p\mathrm{O_2}) = f_{oxt}(t) + f_{oxfb}(p\mathrm{O_2})$, define a summary flux $f_{surf}(t) = f_{met}(t) + f_{mantle}(t) - f_{Cburial}(t) + f_{oxt}(t)$, and rewrite as:

$$f_{redox} = -f_{hesc}\,(p\mathrm{CH_4}) + f_{surf}(t) + f_{oxfb}(p\mathrm{O_2}) \qquad (1).$$

Here $f_{surf}(t)$ represents any time-dependent imbalance between carbon burial $f_{Cburial}$ , metamorphic and mantle inputs, and oxidation $f_{ox}$, treated as an exogenous driver of the system. $f_{oxfb}$ is a parameterization of any oxygen-dependence of carbon burial and oxidation rates. The timescale for equilibration of atmospheric oxygen is long ($\approx 10^6$ yr), hence we explicitly consider the dynamics and stability driven by a combination of stochastic forcing from changes in the carbon burial rate, and slow secular change in $f_{mantle}$.

Time-dependent solutions were derived by integration using a variable-step size Runge-Kutta algorithm (as implemented by the Matlab ode23 function) and steady-state solutions were derived by integrating to convergence.

## 3. Results

### 3.1. Oxygenation of the surface ocean and marine export production

Once the advent of oxygen photosynthesis lifts constraints from electron donor supply (Kharecha et al., 2005), light and nutrients remain as the (abiotic) constraints on productivity. An upper limit on Late Archean surface ocean oxygen concentration [$O_2$] ($\mu$M) (in the absence of methanotrophy) is

then determined by the balance between export production from oxygenic photosynthesis to anoxic depths, *EP* (which represents a net oxygen source to the surface ocean), and escape to the atmosphere represented by piston velocity $\kappa_w$ (m hr$^{-1}$):

$$[O_2]_s \approx 4.7\ (EP\ /\ EP_0)\ /\ (\kappa_w\ /\ \kappa_{w0})\ \mu M \qquad (2)$$

where $EP_0$ = 8.5 mol m$^{-2}$ yr$^{-1}$ is a global mean for highly productive ocean margin regions today and the global mean $\kappa_{w0}$ = 0.2 m hr$^{-1}$.

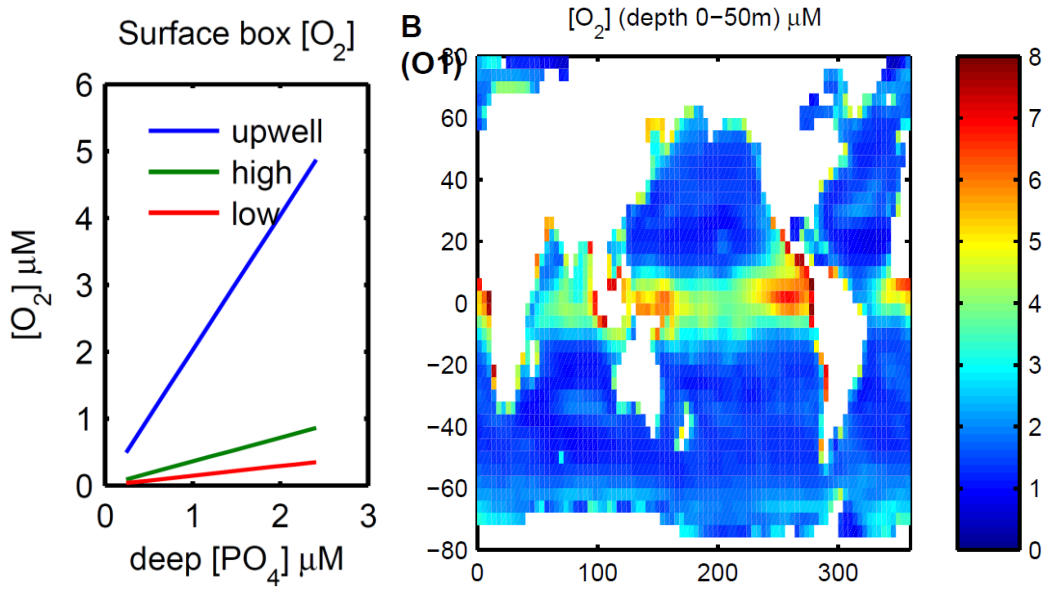


**Figure 2. Upper limit on surface oxygen concentration (in the absence of methanotrophy) with nutrient limited oxygenic photosynthesis and atmospheric oxygen restored to zero. (A) Box model (Supplementary Methods). (B) GCM scenario 'S1' with present-day nutrient level and aerobic respiration occurring in the oxygen oases created (Supplementary Table A-3 and Fig. A-9).**

The primary controls on *EP* are nutrient supply via the combination of nutrient concentration and the ocean circulation, and seasonal light limitation at high latitudes. GCM and box model simulations (Figure 2 and Supplementary Fig. A-9) confirm that the resulting upper limits on surface oxygen concentrations are of the order $[O_2]_s \approx$ 1-10 µM with maxima expected in upwelling regions. We use the present-day continental configuration and ocean circulation because these details and the Late Archean climate are largely unknown. However, the physical processes driving wind-driven

upwelling and stratification will still result in open-ocean wind-driven gyres and hence equatorial and high-latitude upwelling, coastal upwelling regions, and low-latitude stratification with high-latitude seasonal deep mixed-layer depths. *EP* and hence $[O_2]_s$ is approximately proportional to nutrient level (Fig 2A) and nutrient levels are also uncertain (Konhauser et al., 2007), but even nutrient levels as little as 10% of present provide sufficient productivity to support an aerobic ecosystem ($[O_2]_s \approx 1$ μM) in upwelling regions (Supplementary Fig A-12).

*NPP* is a less well constrained multiple of *EP*, as a result of surface-ocean recycling in the microbial loop. This recycling increases predicted NPP (and hence oxygen production) relative to export production by at least a factor of 3 in the contemporary ocean (Laws et al., 2000). Bacterial aerobic growth has been demonstrated down to nanomolar oxygen concentrations (Stolper et al., 2010), with the limiting concentration close to the cellular diffusion limit. We therefore assume that aerobic heterotrophic carbon and nutrient cycling in a microbial loop would have operated with an efficiency at least comparable to that in present-day ecosystems, and potentially larger (limited ultimately by light availability) given the absence of eukaryotic predation to package large sinking particles. Changing the depth dependency of nutrient recycling, such that nutrients are recycled aerobically at shallower depths in a prokaryote-dominated world increases *NPP*. However, as this cycling produces and consumes oxygen in equal measure it leaves *EP* and hence $[O_2]_s$ and balanced fluxes unchanged (Supplementary Table A-3, Section A-5.4).

### 3.2. Biosphere methane cycling

Nutrient, [P], supply to the mixed layer from ocean upwelling and high latitude convection (*U*) determines export production, via a 'Redfield ratio' ($r_{c:p}$). In the Late Archean this export production would have determined the maximum methane flux produced in deeper anoxic layers, setting an upper limit on the balanced fluxes of methane and oxygen that can leave the ocean in the absence of methanotrophy:

$$f_{bal} \leq EP \approx U\,[P]_d\, r_{c:p} \approx 2U\,[CH_4]_d \text{ mol } O_2 \text{ yr}^{-1} \quad (3)$$

Taking modern day [P] = 2.17 μM as an upper limit, $U \approx 100$ Sv (Supplementary Table A-1) and $r_{c:p}$ = 117, typical for modern cyanobacteria, the resulting flux is $\approx 8\times10^{14}$ mol $O_2$ yr$^{-1}$, which is only ≈20% of contemporary NPP. Here we are assuming no alternative electron acceptors in the low sulphur Late Archean environment, but we expect that iron would have contributed (Kharecha et al., 2005). Whilst $r_{c:p}$ could conceivably have been higher or lower in the Late Archean ocean, [P] is generally expected to have been lower, so our upper limit is unlikely to have been exceeded. In the presence of aerobic methanotrophy, $[O_2]_s$ and $[CH_4]_s$ are then reduced to levels above a minimum determined by the limiting concentration required to support methanotrophy, $[O_2]_s \approx 0.01$–$0.1$ μM and $[CH_4]_s < R^*$, where $R^* \leq R^*_0 = 0.1$ μM (Tavormina et al., 2010; Valentine, 2011) (Supplementary Material Section A-1). This limits the rate of methane escape to the atmosphere, leading to a lower limit (assuming local balance of methane and oxygen supply):

$$f_{bal} \geq 1.2\times10^{14}(k_w/k_{w0})(R^*/R^*_0) \text{ mol } O_2 \text{ yr}^{-1} \quad (4)$$

Three mechanisms will increase the atmospheric flux above this limit. Firstly, spatial and temporal decoupling of export production from fermentation and methanogenesis mean that methane and oxygen are not equally available at the redoxcline. Seasonal high-latitude production therefore results in excess summer oxygen production and winter methane escape. Secondly, accumulation and consumption of oxygen over a diel cycle leads to a minimum daily mean concentration $[O_2]_{diel} \approx 0.14$ ($NPP$/10 mol C m$^{-2}$yr$^{-1}$)/($z_{ml}$ / 50 m) μM (Supplementary Material Section A-1.3), where for typical open-ocean values of net primary productivity $NPP$ and mixed layer depth $z_{ml}$ this is a relatively small effect. Third, methane ebullition may result in atmospheric escape of methane produced in sediments. This likely provided a major mechanism in shallow-water environments, as it does today (Valentine, 2011), but we do not include it in our open ocean models.

The effect of methanotrophy and spatial and temporal decoupling on surface oxygen concentration is illustrated using the GCM simulations in Figure 3. Oxygen levels approach the methanotroph-determined limiting concentration at low latitudes (with methane in small excess as a result of spatial decoupling), but are higher at seasonal high latitudes. Crucially, however, aerobic ecosystems are still widespread in the model. The overall pattern of surface oxygen concentration is consistent with previous work (Olson et al., 2013).

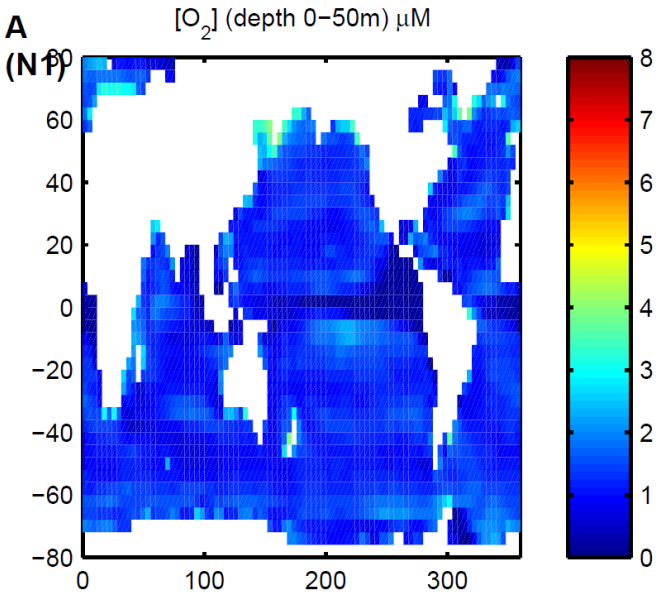


**Figure 3. Annual mean surface oxygen concentration for GCM scenario 'N1', including aerobic methanotrophy.**

Our GCM simulations also predict that roughly 40% of upwelling methane would have been consumed by aerobic methanotrophy in the Late Archean and therefore the balanced flux of methane and oxygen leaving the ocean would have been roughly 60% of export production (Supplementary Table A-3 and Figures A-12). This result is due to a combination of spatial decoupling of methane and oxygen supply in low latitude regions and temporal decoupling in seasonal high latitudes (Supplementary Figures A-10, A-11). The range of balanced flux ≈1-5.7×$10^{14}$ mol $O_2$ $yr^{-1}$ for 0.1–1 modern day nutrient levels is most directly linked to *EP* rather than *NPP* and hence is only ≈20% of that considered in some previous box models (Goldblatt et al., 2006). The fraction of NPP converted to a balanced flux is less well constrained, because NPP depends on the degree of

nutrient cycling within oxygen oases. With a conservative, modern day assumption that around two-thirds of NPP is recycled and one-third is exported to depth, the balanced flux is about one-fifth of NPP (Figure 4). The balanced flux range considered here includes the $4.0\times10^{14}$ mol $O_2$ $yr^{-1}$ assumed by Claire et al. (2006) and the $2.0\times10^{14}$ mol $O_2$ $yr^{-1}$ assumed by Catling et al. (2007).

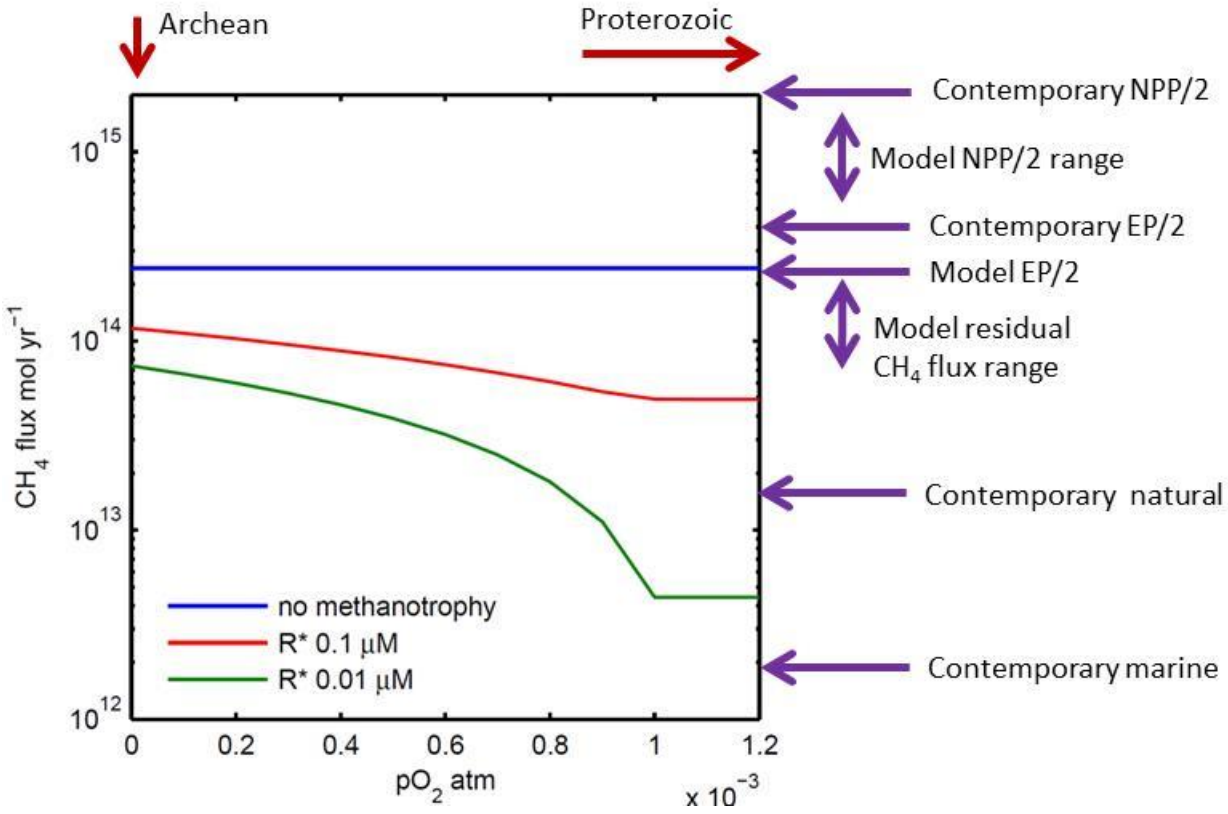


**Figure 4. Atmospheric methane fluxes (0.5 $f_{bal}$) from the marine biosphere box model, compared to contemporary fluxes and demonstrating the effect of increase in atmospheric oxygen to Proterozoic levels following the Great Oxidation. Net oxygen and methane production from the oxygenated surface layer is most directly related to export production *EP*. The balanced flux escaping to the atmosphere is reduced below *EP* by aerobic methanotrophy, depending on limiting oxygen and methane concentration (*R**). The advent of atmospheric oxygen provides an additional oxygen transport pathway, supporting additional consumption by aerobic methanotrophy and reducing $f_{bal}$.**

### 3.3. Effect on the Great Oxidation

The two existing models for the Great Oxidation transition while demonstrating the same overall redox control on atmospheric oxygen, and highly non-linear response, differ in the assumed biosphere methane/oxygen balanced flux, and in the driving mechanism included. The model of

315 Goldblatt et al. (2006) assumed nearly all NPP translates into a balanced flux (with a parameterized
316 decline in balanced flux with increasing atmospheric $pO_2$, Figure 5B), and generated a bistable
317 transition with two atmospheric oxygen states available for a range of Earth-surface reductant input.
318 The model of Claire et al. (2006) argued for a lower biosphere flux of $2.0\times10^{14}$ mol $O_2$ $yr^{-1}$ and also
319 calculated the effect of hydrogen escape on oxidation of the crust, and hence the redox state of
320 metamorphic flux and the secular evolution of atmospheric oxygen. Our approach here is to
321 examine the effect of the balanced flux of methane and oxygen on the Great Oxidation transition,
322 while prescribing the time-dependent evolution of Earth-surface redox input as a forcing parameter.

323

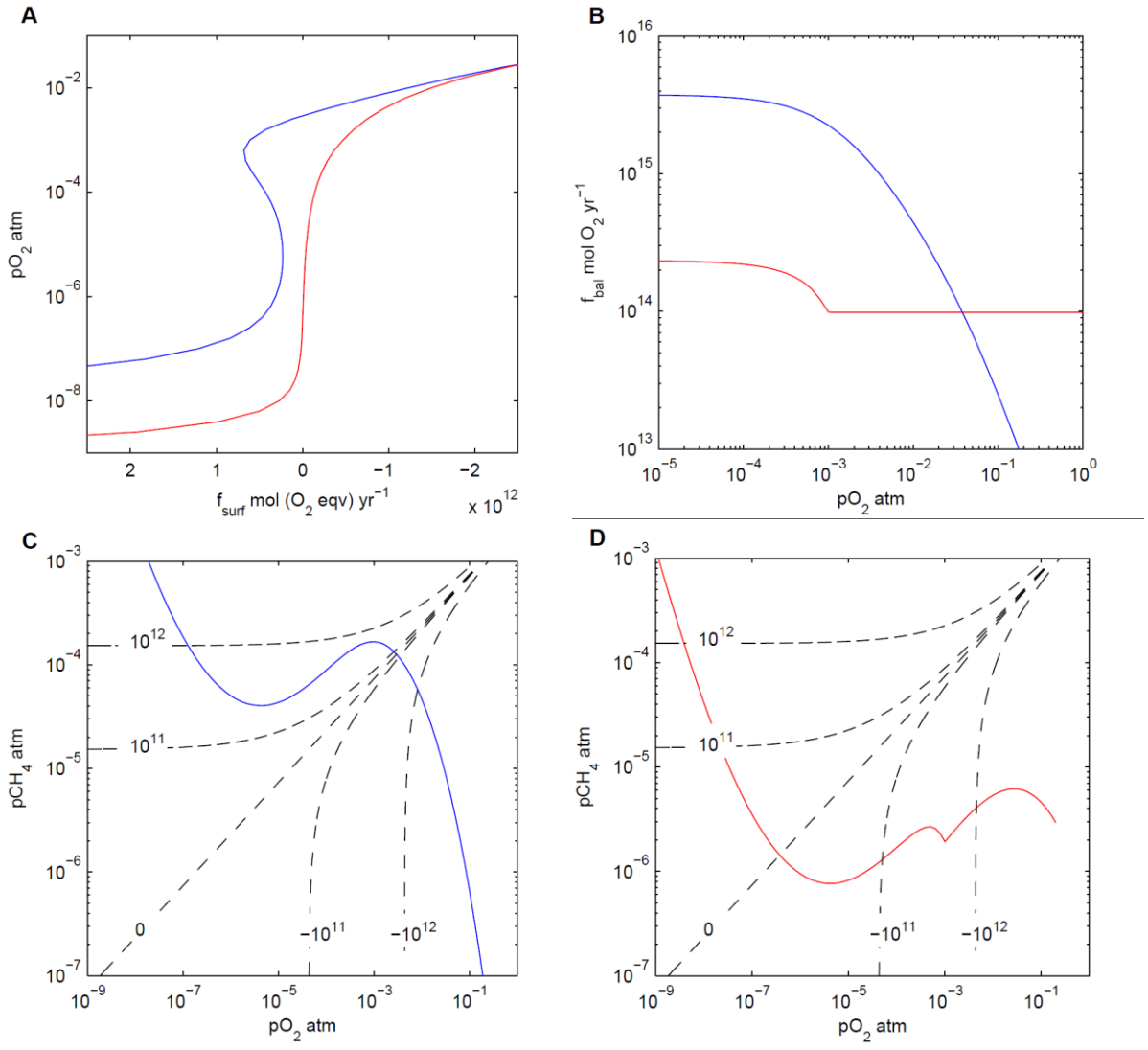


**Figure 5. Controls on atmospheric stability. (A) Steady state solutions for $pO_2$ as a function of reductant input $f_{surf}$, for two models for oxygen/methane balanced flux. Blue corresponds to the model of Goldblatt et al. (2006), with $f_{bal} = N\Omega_{O2}$ where $N = 3.75\times10^{15}$ mol $O_2$ $yr^{-1}$ is NPP and $\Omega_{O2}(pO_2)$ is a parameterized decrease with increasing $pO_2$. Red is for the box model shown in Figure 4 with $R^*$=0.1 µM and $f_{bal} = 2.3\times10^{14}$ mol $O_2$ $yr^{-1}$ at low $pO_2$ decreasing to $1.0\times10^{14}$ mol $O_2$ $yr^{-1}$ at high $pO_2$. (B) Corresponding values of the balanced flux of methane and oxygen escaping the ocean. The revised lower value of balanced flux eliminates the bistability of $pO_2$. (C) Phase space portrait for the model of Goldblatt et al. (2006) where dashed lines are values of $f_{surf} + f_{oxfb}$ with $f_{surf} = 10^{12}$, $10^{11}$, 0, $-10^{11}$, $-10^{12}$ mol $O_2$ equiv $yr^{-1}$ as indicated. (D) Phase space portrait for the marine biosphere box model. See Supplementary Fig A4, A6 for additional sensitivity studies.**

We first consider the steady state solutions for atmospheric oxygen concentration (Figure 5A). The high balanced-flux case (Goldblatt et al., 2006) produces a broad region of bi-stability for $O_2$,

whereas with our revised estimate including aerobic recycling in the surface ocean, the bi-stability is eliminated leaving a sharp non-linear transition.

The non-linearity of the atmospheric transition is due to the effect of the formation of the ozone layer on the atmospheric photochemical methane oxidation rate (Claire et al., 2006; Goldblatt et al., 2006). There is a positive feedback regime in which as the ozone layer starts to form, this suppresses oxygen consumption, accelerating ozone accumulation, and this tends to separate low and high stable states for oxygen. However, the degree of bi-stability or hysteresis also depends on the strength of the negative feedback involving hydrogen escape to space (an oxygen source). This is particularly important in the high oxygen state: if some factor tends to reduce the oxygen concentration, this generates a counterbalancing increase in methane concentration and hydrogen escape, which resists the initial change. With a lower balanced flux of methane and oxygen, the methane concentration and hydrogen escape rate are lower, hence the negative feedback is weaker. Thus, reducing the balanced flux of oxygen and methane from the ocean (Figure 5B) shrinks the basin of attraction of the high oxygen state and suppresses the bi-stability (Figure 5A).

The controls on atmospheric stability can be further understood by considering the phase space of oxygen and methane concentrations (Figure 5C,D). Here solutions for the original model with high balanced flux (Figure 5C) and the new model with low balanced flux (Figure 5D) are intersected by different functions for the net Earth surface input of reductant ($f_{surf} + f_{oxfb}$) to the atmosphere (or oxidant input if the value is negative). These dashed lines correspond to different fixed values of $f_{surf}$ but are curved because $f_{oxfb}$ is sensitive to atmospheric composition. In the original model, with a high balanced flux (Figure 5C), the oxygen source from hydrogen escape can still exceed the sink from oxidative weathering for $pO_2 < 10^{-3}$ atm. This allows two steady states to exist for $f_{surf} = 0.25–0.7\times10^{12}$ mol $O_2$ equiv $yr^{-1}$, in both of which net reductant input is balanced by hydrogen escape to space. In contrast, in the new model with low balanced flux (Figure 5D) there is only ever one steady state. This oxygen-methane steady-state in Figure 5D is similar to that of Claire et al. (2006) and

Zahnle et al. (2006), as our balanced flux is comparable to what they assume (see Supplementary Section A-3 for additional comparison and sensitivity studies). We note that the high balanced flux from Goldblatt et al. (2006) exceeds the upper limit of $2.7 \times 10^{15}$ mol $O_2$ $yr^{-1}$ considered by Zahnle et al. (2006) hence Fig 5C is in their 'inaccessible region'.

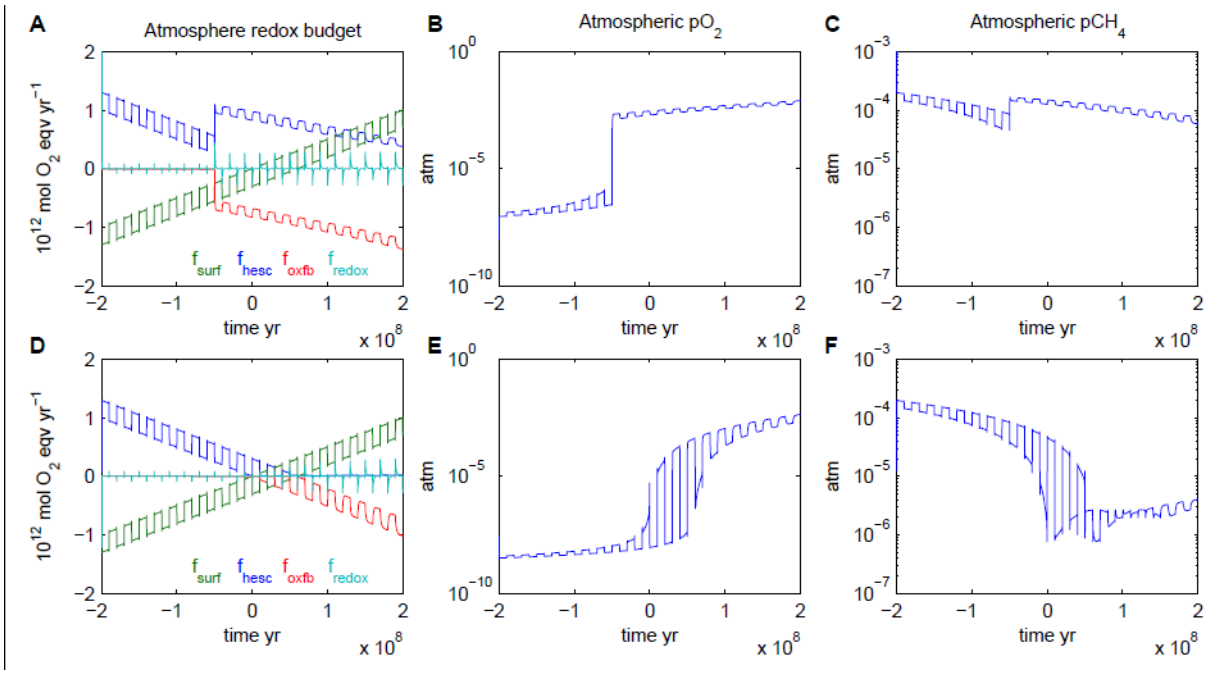


**Figure 6. Atmosphere evolution for the two models for oxygen/methane balanced flux described in Figure 5: (A,B,C) the model of Goldblatt et al. (2006) with $f_{bal} = N\Omega_{O2}$ where $N = 3.75 \times 10^{15}$ mol $O_2$ $yr^{-1}$ is NPP, and (D,E,F) the box model shown in Figure 4 with $R^*$=0.1 µM. Left panels (A,D) show components of overall net reductant input, $f_{redox}$ as defined by Equation (1). The models are forced by a secular decrease in reductant input representing a slow overall oxidation of the Earth surface, and an pulsed imbalance between carbon burial and oxidative weathering of $\pm 1.5 \times 10^{11}$ mol $O_2$ $yr^{-1}$ with time period 20 My. Time zero corresponds to $f_{surf} = 0$ (cf $K_{OXY} = 0$ in Claire et al. 2006).**

This is explored further with two scenarios for atmospheric evolution (Figure 6) based on the same pair of models for balanced methane/oxygen flux, from NPP (Goldblatt et al., 2006) and our revised lower estimate. The Earth surface reductant input $f_{surf}$ is treated as an exogenous time-dependent forcing term, representing both a stochastic imbalance between carbon burial, metamorphic and volcanic inputs, and oxidative weathering (a pulsed input of $\pm 1.5 \times 10^{11}$ mol $O_2$ $yr^{-1}$ and time period 20

My), and a secular decrease in reductant input representing a slow overall oxidation of the Earth surface.

As a function of time, atmosphere evolution shows three regimes (Claire et al., 2006): (i) Prior to the Great Oxidation, the atmosphere is in a stable, steady-state regime with methane level set by a balance between reductant input and hydrogen escape, hence the two scenarios show the same methane concentration. Oxygen is a trace gas, with concentration is set to balance oxygen input and atmospheric oxidation, and is therefore lower in the lower balanced flux scenario. (ii) During the transition to an oxic atmosphere, the atmosphere is in a non-steady state with falling methane and rising oxygen levels, and methane/oxygen balance is controlled by the short-timescale atmospheric methane oxidation process. As oxygen levels rise, methane levels must drop (Zahnle et al., 2006) and pass through a minimum at $pO_2 \sim 10^{-5}$ atm (Fig A-3) determined only by the balanced flux input, hence minimum methane level is lower in the low balanced flux scenario. Hydrogen escape feedback stabilises the high oxygen state in the high balanced flux scenario, whereas in the low balanced flux scenario the imposed tectonic forcing of reductant input drives multiple transitions in atmospheric oxygen. (iii) After the Great Oxidation, the atmosphere approaches a higher oxygen steady-state, where the oxygen level is set by oxygen-sensitive oxidative weathering balancing reductant input. Methane is the trace gas, and the methane level is set by balancing methane input and atmospheric oxidation. Hence methane concentration is much lower in the low balanced flux scenario, and hydrogen escape is correspondingly much smaller in this scenario than in the high balanced flux case.

The increase in atmospheric oxygen concentration following the Great Oxidation would have further reduced the marine methane flux (Figure 4, Figure 5B), because oxygen redistribution via the atmosphere would have compensated for the spatial decoupling of methanogenesis from marine oxygen production, bringing oxygen to where methane was available for consumption by methanotrophs. An estimated lower limit on Proterozoic $pO_2 \approx 0.01$ PAL (Rye and Holland, 1998) is

comparable to the atmospheric oxygen concentration (set by transport limitation at the air-sea interface) that would have been sufficient to prevent oxygen limitation of methanotrophy (Figure 3). Hence the flux of methane 0.5 $f_{bal}$ from the ocean in the early Proterozoic could have been reduced to the limit given by Equation (4), which assuming $R^*$ = 0.01 μM is near the contemporary marine flux (Figure 4). As in the present, methane flux would then have been dominated by shallow water wetlands (Figure 4). This results in a methane concentration of ≈1–5 ppm and represents a Phanerozoic type of methane control where surface input is balanced by atmospheric oxidation.

### 3.4. $\delta^{13}C_{org}$ signature of methane cycling

A key test of the hypothesis of abundant aerobic methanotrophy in oxygen oases before the Great Oxidation are its predicted effects on the $\delta^{13}C_{org}$ record (Eigenbrode and Freeman, 2006; Hayes, 1994). The key control on the local isotopic composition $\delta^{13}C_{org}$ of sedimentary organic carbon is the ratio of primary autotrophic production ($\delta^{13}C_{org}$ ≈ -30 ‰) to secondary methanotroph production ($\delta^{13}C_{org}$ <-70 ‰) in the organic carbon supply. In the limit where all autotroph production is locally recycled, methanotroph growth efficiency $g_m$ = 1, and *EP* is high so atmospheric escape is negligible, $\delta^{13}C_{org}$ will approach $\delta_p - \varepsilon_m/2$ ≈ -70 ‰ where $\varepsilon_m$ ≈ 80 ‰ is the fractionation produced by fermentation and methanogenesis (Hayes, 1994). However, realistic methanotroph growth efficiencies are $g_m$ < 0.5, and the fraction of export production reprocessed via methanotrophy is further reduced by spatial/temporal imbalances between export production and methanotropy, and by atmospheric escape.

The combination of these factors in our models leads to predictions of $\delta^{13}C_{org}$ ranging over ≈-30 to -45 ‰ (Figure 7), which are consistent with most deeper water data from 2.65–2.45 Ga (Eigenbrode and Freeman, 2006; Fischer et al., 2009). The models give the lowest $\delta^{13}C_{org}$ of sinking organic matter where upwelling nutrients fuel the most productive communities and oxygen oases. In oligotrophic gyres, $\delta^{13}C_{org}$ remains close to that of photosynthetic matter, because little aerobic methanotrophy can be supported. To reproduce the most extreme inferred deeper water $\delta^{13}C_{org}$ ≈-50 ‰ (from 2.65–

427 2.6 Ga) requires extreme assumptions, e.g. that methanotrophs have growth efficiency $g_m = 1$

428 allowing them to convert all the methane available to them in upwelling zones into biomass

429 (Supplementary Fig. A-14).

430

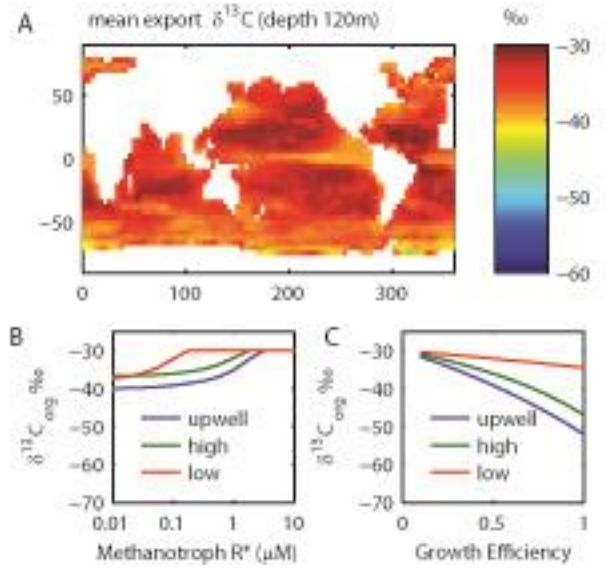


431

432 **Figure 7. Predicted $\delta^{13}C$ of sinking organic matter. (A) GCM scenario 'G1' with methanotroph growth efficiency 0.5**

433 **(Supplementary Methods). Box model dependency on (B) methanotroph limiting oxygen and methane concentration,**

434 **and (C) growth efficiency, for upwelling, high-latitude and low-latitude surface boxes.**

435 **4. Discussion**

436 **4.1 Geochemical signature of marine aerobic ecosystems**

437 By ≈2.6 Ga (if not before) oxygenic photosynthesis was creating oxygen oases in the open ocean

438 (Czaja et al., 2012), which fuelled aerobic ecosystems including methanotrophs that produced $\delta^{13}C_{org}$

439 ≈-30 to -50 ‰ in deeper sediments (Eigenbrode and Freeman, 2006). We suggest the most negative

440 $\delta^{13}C_{org}$ could have been produced in shelf-slope upwelling regions, where upwelling methane-rich

441 water met oxic shelf water concentrating methanotroph production (Figure 8A).

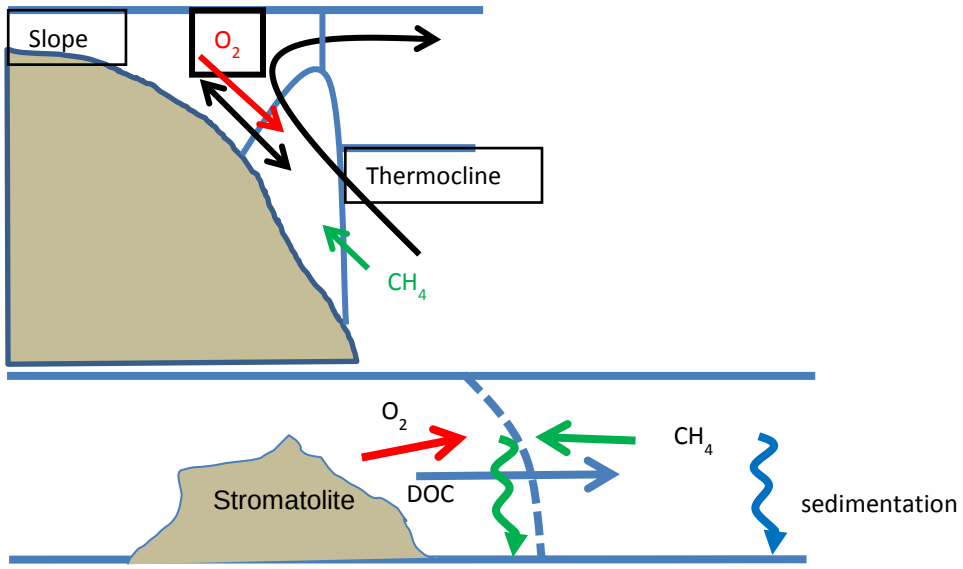


**Figure 8. Two scenarios for the generation of extremely isotopically light $\delta^{13}C_{org}$ through the spatial concentration of aerobic methanotrophy. (A) Shelf-slope upwelling region. (B) Microbial mat scenario.**

$\delta^{13}C_{org}$ values become generally less negative 2.6–2.45 Ga on approaching the Great Oxidation (Eigenbrode and Freeman, 2006). This could have been because increasing sulphur concentration due to sulphur input from oxidative weathering caused the spread of anaerobic oxidation of methane (AOM), at the expense of aerobic methanotrophy. Sulphate provides an electron shuttle across the redoxcline, which would initially have driven a fraction of methane consumption to deeper depths in the water column – as seen in low-sulphate contemporary Lake Tanganyika (Durisch-Kaiser et al., 2011). Ultimately, rising sulphate concentrations would have driven methane consumption into the sediments, as assumed by Catling et al. (2007). AOM has low growth efficiency (Hinrichs, 2002), hence its spread would have reduced the contribution of methanotroph biomass to sedimentary organic carbon, producing less negative $\delta^{13}C_{org}$. Alternatively, as sulphate built up in the ocean, sulphate reducers could have out-competed methanogens for sinking organic matter and out-competed anaerobic methane oxidisers for sulphate, tending to reduce the cycling of carbon through methanotrophs and thus produce less negative $\delta^{13}C_{org}$.

Increasing sulphur and AOM would have provided an additional redox shuttle and oxidant buffer within the water column and sediments, potentially further reducing the atmospheric methane flux

(Beal et al., 2011; Catling et al., 2007). For example, a marine sulphate concentration of ~100 μM would be sufficient to buffer high-latitude seasonality (lack of oxygen production over winter) effectively turning a methane atmospheric flux into sulphide. However, our central result is unaffected; this methane flux, and the associated balanced oxygen flux, would have been relatively low, due to oxygen and methane cycling within the ocean, making the Great Oxidation more reversible and probably episodic in nature. Our low balanced flux estimate (e.g. $2.3\times10^{14}$ mol $O_2$ $yr^{-1}$ at low $pO_2$ in Figures 4 and 5) is close to that assumed by Catling et al. (2007) in the presence of sedimentary AOM ($2.0\times10^{14}$ mol $O_2$ $yr^{-1}$), and below that assumed by Claire et al. (2006) ($4.0\times10^{14}$ mol $O_2$ $yr^{-1}$). These authors' alternative model can also show an episodic rise of atmospheric $O_2$ at the Great Oxidation in the presence of climate feedbacks (Claire et al., 2006), consistent with oxygen rise being more reversible in a low balanced flux scenario.

### 4.2 Microbial mat systems and their geochemical signature

A complementary model of the Late Archean and Proterozoic world is that microbial mats in shallow waters and on the land surface were major players in the cycling of oxygen and methane. Cyanobacterial phylogeny suggests a freshwater origin for oxygenic photosynthesis (Blank and Sánchez-Baracaldo, 2009), consistent with the interpretation that it was occurring in shallow water lacustrine or estuarine environments, recorded in the Tumbiana formation at 2.72 Ga (Buick, 1992). These same 2.72 Ga sediments host the most negative $\delta^{13}C_{org} \approx$ -60 ‰ (Eigenbrode and Freeman, 2006), which cannot be reproduced under realistic assumptions in our open ocean models. The signal probably reflects methanotrophy at the edges of shallow-water stromatolites (Thomazo et al., 2009), where oxygen from microbial mats meets methane produced from exported dissolved organic carbon (DOC) (Figure 8B) allowing methanotroph secondary production to locally dominate the biomass. This is consistent with the isotopically light $\delta^{13}C_{org}$ being located in mudstones, not just stromatolites (Thomazo et al., 2009).

Atmospheric fluxes from microbial mat systems would have depended on spatial and temporal decoupling of oxygenic photosynthesis and carbon cycling, as in the pelagic marine ecosystem. Benthic mats where water depth exceeds ~5m (the air-sea exchange piston velocity in m $d^{-1}$) would have been buffered against daily atmospheric exchange by oxygen accumulation and consumption in the water column. However mats in land-surface or intertidal environments (Lalonde and Konhauser, 2015) could have provided an atmospheric oxygen and reduced gas source over a diel cycle. The median net daytime oxygen production rate (0.16 nmol $cm^{-2}$ $s^{-1}$) from the compilation of Lalonde and Konshauser (2015), with a 50% correction for diel cycle mean and integrated over a modern wetland area of $10^7$ $km^2$ (~7% of land area) corresponds to a global annual flux of $2.5x10^{14}$ mol $O_2$ $yr^{-1}$. However direct measurements of mat fluxes under anoxic conditions (which restricts oxidant availability hence may limit night-time carbon and hence nutrient recycling) are scarce. Hoehler et al. (2001) measured reduced flux (hydrogen) over a diel cycle from an intertidal mat under laboratory anoxic conditions equivalent to $3.2x10^{13}$ mol $O_2$ eq $yr^{-1}$ when scaled to 10% of contemporary marine NPP (their Table 2).

**4.3 Controls on Archean methanotrophy and atmospheric oxygen and methane.**

Sulphur isotope data show correlations between changes in the mass-independent fractionation $\Delta^{36}S/\Delta^{33}S$ slope and negative $\delta^{13}C_{org}$ excursions at multiple locations (2.65 Ga Ghaap Group and ~2.5 Ga Gamohaan Formation, South Africa, ~2.5 Ga Mount McRae Shale and ~2.7 Ga Tumbiana Formation, Western Australia) (Zerkle et al., 2012). This was interpreted as the result of transiently increased biogenic methane production increasing both methanotropy, and atmospheric methane concentration leading to the formation of organic haze with corresponding changes in atmospheric sulphur exit channels.

However, we find in our atmospheric model that an increase in balanced flux – nominally due to an increase in productivity, methanogenesis and methanotrophy – leaves atmospheric $pCH_4$ unchanged and increases $pO_2$ (and in fact would be likely to also generate increased carbon burial hence reduce

510 $pCH_4$). In contrast, an increase in reductant input – plausibly driven by a tectonic volcanic or
511 metamorphic perturbation – increases $pCH_4$ and reduces $pO_2$. We therefore suggest that
512 correlations between $\delta^{13}C_{org}$ and sulphur MIF are more likely to be the result of tectonic
513 perturbations, with a reductant input (volcanic or metamorphic methane production) increasing
514 $pCH_4$, and an accompanying methane or $CO_2$-driven temperature, weathering and nutrient supply
515 increase driving increased productivity and methanotrophy.

516 **4.4 Proterozoic methane**

517 In the aftermath of the Great Oxidation, we predict a reduction in the methane flux from the ocean
518 to the Proterozoic atmosphere to $\approx 1.0\times10^{14}$ mol $O_2$ $yr^{-1}$, because oxygen was no longer limiting to
519 aerobic methane consumption anywhere in the surface ocean. Atmospheric methane input in the
520 Proterozoic was likely dominated instead by shallow-water and mat-based environments – just as
521 contemporary net biospheric methane production is dominated by wetlands. However, this
522 methane flux would have been reduced by sulphate input. Our estimate of post-Great Oxidation
523 methane flux is an order-of-magnitude less than the $7.5\text{-}15\times10^{14}$ mol $O_2$ $yr^{-1}$ suggested in arguments
524 for a methane-rich Proterozoic atmosphere (Pavlov et al., 2003; Roberson et al., 2011). Hence rather
525 than 100 ppm of $CH_4$ in the Proterozoic atmosphere (Pavlov et al., 2003; Roberson et al., 2011), we
526 predict <10 ppm (Figure 6F). The warming potential of methane was originally over-estimated
527 (Pavlov et al., 2003) due to an error in the model code (Byrne and Goldblatt, 2014; Roberson et al.,
528 2011). Lowering $CH_4$ concentration by at least an order-of-magnitude further adds to the problem of
529 explaining Proterozoic warmth, suggesting that a combination of $CH_4$, $N_2O$ and $CO_2$ (Roberson et al.,
530 2011) is not sufficient and other contributions should be considered (Byrne and Goldblatt, 2014). A
531 low Proterozoic methane concentration also suggests ongoing hydrogen escape would have been
532 modest and is unlikely to have greatly reinforced the transition to a permanently oxic atmosphere.
533 Instead, other feedback mechanisms must have made the Great Oxidation permanent, such as land-

surface oxidative weathering of nutrients fuelling marine productivity and organic carbon burial (Bekker and Holland, 2012).

### 4.5 Further work

The scenario of widespread oxygen oases prior to the Great Oxidation can be further tested. One route would be to simulate the combined effects of our revised Late Archean oxygen and methane fluxes on the MIF of S signature (Claire et al., 2014). A potentially strong constraint on the degree of oxygenation of the surface ocean could come from process-based models of sulphur species oxygenation in the water column (Halevy, 2013).

Our results demonstrate that quantitatively representing carbon, oxygen and methane cycling within the marine environment is key to both interpreting the organic carbon isotope record, and to understanding the evolution and stability of atmospheric composition. Future work should extend this approach to quantify the relationship between marine redox-sensitive proxies and the oxidation state of the water column (which is only indirectly coupled to atmospheric oxidation state), to include microbial mats and understand their contribution to oxygen and methane cycling, and to test hypotheses for Earth-system-level feedbacks during and after the Great Oxidation, including the role of climate feedbacks.

## References

Beal, E.J., Claire, M.W., House, C.H., 2011. High rates of anaerobic methanotrophy at low sulfate concentrations with implications for past and present methane levels. Geobiology 9, 131-139.

Bekker, A., Holland, H.D., 2012. Oxygen overshoot and recovery during the early Paleoproterozoic. Earth and Planetary Science Letters 317-318, 295-304.

556 Blank, C.E., Sánchez-Baracaldo, P., 2009. Timing of morphological and ecological innovations in the
557 cyanobacteria – a key to understanding the rise in atmospheric oxygen. Geobiology 8, 1-23.

558 Buick, R., 1992. The Antiquity of Oxygenic Photosynthesis: Evidence from Stromatolites in Sulphate-
559 Deficient Archaean Lakes. Science 255, 74-77.

560 Byrne, B., Goldblatt, C., 2014. Radiative forcings for 28 potential Archean greenhouse gases. Clim.
561 Past 10, 1779-1801.

562 Catling, D.C., Claire, M.W., Zahnle, K.J., 2007. Anaerobic methanotrophy and the rise of atmospheric
563 oxygen. Phil. Trans. B 365, 1867-1888.

564 Claire, M.W., Catling, D.C., Zahnle, K.J., 2006. Biogeochemical modelling of the rise in atmospheric
565 oxygen. Geobiology 4, 239-269.

566 Claire, M.W., Kasting, J.F., Domagal-Goldman, S.D., Stüeken, E.E., Buick, R., Meadows, V.S., 2014.
567 Modeling the signature of sulfur mass-independent fractionation produced in the Archean
568 atmosphere. Geochimica et Cosmochimica Acta 141, 365-380.

569 Crowe, S.A., Dossing, L.N., Beukes, N.J., Bau, M., Kruger, S.J., Frei, R., Canfield, D.E., 2013.
570 Atmospheric oxygenation three billion years ago. Nature 501, 535-538.

571 Crowe, S.A., Paris, G., Katsev, S., Jones, C., Kim, S.-T., Zerkle, A.L., Nomosatryo, S., Fowle, D.A.,
572 Adkins, J.F., Sessions, A.L., Farquhar, J., Canfield, D.E., 2014. Sulfate was a trace constituent of
573 Archean seawater. Science 346, 735-739.

574 Czaja, A.D., Johnson, C.M., Roden, E.E., Beard, B.L., Voegelin, A.R., Nägler, T.F., Beukes, N.J., Wille,
575 M., 2012. Evidence for free oxygen in the Neoarchean ocean based on coupled iron–molybdenum
576 isotope fractionation. Geochimica et Cosmochimica Acta 86, 118-137.

David, L.A., Alm, E.J., 2011. Rapid evolutionary innovation during an Archaean genetic expansion. Nature 469, 93-96.

Durisch-Kaiser, E., Schmid, M., Peeters, F., Kipfer, R., Dinkel, C., Diem, T., Schubert, C.J., Wehrli, B., 2011. What prevents outgassing of methane to the atmosphere in Lake Tanganyika? Journal of Geophysical Research: Biogeosciences 116, G02022.

Eigenbrode, J.L., Freeman, K.H., 2006. Late Archean rise of aerobic microbial ecosystems. Proceedings of the National Academy of Sciences 103, 15759-15764.

Farquhar, J., Zerkle, A., Bekker, A., 2011. Geological constraints on the origin of oxygenic photosynthesis. Photosynthesis Research 107, 11-36.

Fischer, W.W., Schroeder, S., Lacassie, J.P., Beukes, N.J., Goldberg, T., Strauss, H., Horstmann, U.E., Schrag, D.P., Knoll, A.H., 2009. Isotopic constraints on the Late Archean carbon cycle from the Transvaal Supergroup along the western margin of the Kaapvaal Craton, South Africa. Precambrian Research 169, 15-27.

Goldblatt, C., Lenton, T.M., Watson, A.J., 2006. Bistability of atmospheric oxygen and the great oxidation. Nature 443, 683-686.

Guy, B.M., Ono, S., Gutzmer, J., Kaufman, A.J., Lin, Y., Fogel, M.L., Beukes, N.J., 2012. A multiple sulfur and organic carbon isotope record from non-conglomeratic sedimentary rocks of the Mesoarchean Witwatersrand Supergroup, South Africa. Precambrian Research 216–219, 208-231.

Halevy, I., 2013. Production, preservation, and biological processing of mass-independent sulfur isotope fractionation in the Archean surface environment. Proceedings of the National Academy of Sciences 110, 17644-17649.

598 Haqq-Misra, J., Kasting, J.F., Lee, S., 2011. Availability of O2 and H2O2 on Pre-Photosynthetic Earth.
599 Astrobiology 11, 293-302.

600 Hayes, J.M., 1983. Geochemical evidence bearing on the origin of aerobiosis, a speculative
601 hypothesis, in: Schopf, J.W. (Ed.), Earth's Earliest Biosphere, Its origin and Evolution. Princeton
602 University Press, Princeton, pp. 291-301.

603 Hayes, J.M., 1994. Global methanotrophy at the Archean-Proterozoic transition, in: Bengtson, S.
604 (Ed.), Early Life on Earth. Columbia University Press, New York, pp. 220-236.

605 Herman, E.K., Kump, L.R., 2005. Biogeochemistry of microbial mats under Precambrian
606 environmental conditions: a modelling study. Geobiology 3, 77-92.

607 Hinrichs, K.-U., 2002. Microbial fixation of methane carbon at 2.7 Ga: Was an anaerobic mechanism
608 possible? Geochemistry, Geophysics, Geosystems 3, 1-10.

609 Hoehler, T.M., Bebout, B.M., Des Marais, D.J., 2001. The role of microbial mats in the production of
610 reduced gases on the early Earth. Nature 412, 324-327.

611 Kasting, J.F., 1991. Box models for the evolution of atmospheric oxygen: an update. Global and
612 Planetary Change 97, 125-131.

613 Kasting, J.F., 2013. What caused the rise of atmospheric O2? Chemical Geology 362, 13-25.

614 Kendall, B., Reinhard, C.T., Lyons, T.W., Kaufman, A.J., Poulton, S.W., Anbar, A.D., 2010. Pervasive
615 oxygenation along late Archaean ocean margins. Nature Geosci 3, 647-652.

616 Kharecha, P., Kasting, J., Siefert, J., 2005. A coupled atmosphere–ecosystem model of the early
617 Archean Earth. Geobiology 3, 53-76.

618 Konhauser, K.O., Lalonde, S.V., Amskold, L., Holland, H.D., 2007. Was There Really an Archean
619 Phosphate Crisis? Science 315, 1234.

620 Kopp, R.E., Kirschvink, J.L., Hilburn, I.A., Nash, C.Z., 2005. The Paleoproterozoic snowball Earth: A
621 climate disaster triggered by the evolution of oxygenic photosynthesis. Proceedings of the National
622 Academy of Sciences of the United States of America 102, 11131-11136.

623 Lalonde, S.V., Konhauser, K.O., 2015. Benthic perspective on Earth's oldest evidence for oxygenic
624 photosynthesis. Proceedings of the National Academy of Sciences 112, 995-1000.

625 Laws, E.A., Falkowski, P.G., Smith, W.O., Ducklow, H., McCarthy, J.J., 2000. Temperature effects on
626 export production in the open ocean. Global Biogeochemical Cycles 14, 1231-1246.

627 Olson, S.L., Kump, L.R., Kasting, J.F., 2013. Quantifying the areal extent and dissolved oxygen
628 concentrations of Archean oxygen oases. Chemical Geology 362, 35-43.

629 Pavlov, A.A., Hurtgen, M.T., Kasting, J.F., Arthur, M.A., 2003. Methane-rich Proterozoic atmosphere?
630 Geology 31, 87-90.

631 Planavsky, N.J., Asael, D., Hofmann, A., Reinhard, C.T., Lalonde, S.V., Knudsen, A., Wang, X., Ossa
632 Ossa, F., Pecoits, E., Smith, A.J.B., Beukes, N.J., Bekker, A., Johnson, T.M., Konhauser, K.O., Lyons,
633 T.W., Rouxel, O.J., 2014. Evidence for oxygenic photosynthesis half a billion years before the Great
634 Oxidation Event. Nature Geosci 7, 283-286.

635 Reinhard, C.T., Raiswell, R., Scott, C., Anbar, A.D., Lyons, T.W., 2009. A Late Archean Sulfidic Sea
636 Stimulated by Early Oxidative Weathering of the Continents. Science 326, 713-716.

637 Riding, R., Fralick, P., Liang, L., 2014. Identification of an Archean marine oxygen oasis. Precambrian
638 Research 251, 232-237.

639 Roberson, A.L., Roadt, J., Halevy, I., Kasting, J.F., 2011. Greenhouse warming by nitrous oxide and
640 methane in the Proterozoic Eon. Geobiology 9, 313-320.

641 Rye, R., Holland, H.D., 1998. Paleosols and the evolution of atmospheric oxygen: A critical review.
642 American Journal of Science 298, 621-672.

643 Siebert, C., Kramers, J.D., Meisel, T., Morel, P., NÃ¤gler, T.F., 2005. PGE, Re-Os, and Mo isotope
644 systematics in Archean and early Proterozoic sedimentary systems as proxies for redox conditions of
645 the early Earth. Geochimica et Cosmochimica Acta 69, 1787-1801.

646 Stolper, D.A., Revsbech, N.P., Canfield, D.E., 2010. Aerobic growth at nanomolar oxygen
647 concentrations. Proceedings of the National Academy of Sciences 107, 18755-18760.

648 Tavormina, P.L., Ussler, W., Joye, S.B., Harrison, B.K., Orphan, V.J., 2010. Distributions of putative
649 aerobic methanotrophs in diverse pelagic marine environments. ISME J 4, 700-710.

650 Thomazo, C., Ader, M., Farquhar, J., Philippot, P., 2009. Methanotrophs regulated atmospheric sulfur
651 isotope anomalies during the Mesoarchean (Tumbiana Formation, Western Australia). Earth and
652 Planetary Science Letters 279, 65-75.

653 Towe, K.M., 1990. Aerobic respiration in the Archaean? Nature 348, 54-56.

654 Valentine, D.L., 2011. Emerging Topics in Marine Methane Biogeochemistry. Annual Review of
655 Marine Science 3, 147-171.

656 Wang, M., Jiang, Y.-Y., Kim, K.M., Qu, G., Ji, H.-F., Mittenthal, J.E., Zhang, H.-Y., Caetano-Anollés, G.,
657 2011. A Universal Molecular Clock of Protein Folds and Its Power in Tracing the Early History of
658 Aerobic Metabolism and Planet Oxygenation. Molecular Biology and Evolution 28, 567-582.

659 Wille, M., Kramers, J.D., Nagler, T.F., Beukes, N.J., Schroder, S., Meisel, T., Lacassie, J.P., Voegelin,
660 A.R., 2007. Evidence for a gradual rise of oxygen between 2.6 and 2.5 Ga from Mo isotopes and Re-
661 PGE signatures in shales. Geochimica et Cosmochimica Acta 71, 2417-2435.

662 Zahnle, K., Claire, M., Catling, D., 2006. The loss of mass-independent fractionation in sulfur due to a
663 Palaeoproterozoic collapse of atmospheric methane. Geobiology 4, 271-283.

664 Zerkle, A.L., Claire, M.W., Domagal-Goldman, S.D., Farquhar, J., Poulton, S.W., 2012. A bistable
665 organic-rich atmosphere on the Neoarchaean Earth. Nature Geosci 5, 359-363.

666 Zhelezinskaia, I., Kaufman, A.J., Farquhar, J., Cliff, J., 2014. Large sulfur isotope fractionations
667 associated with Neoarchean microbial sulfate reduction. Science 346, 742-744.

668

669 **Acknowledgments**

670 We thank James Clark for input to the modelling, and Mark Claire and Colin Goldblatt for thoughtful
671 reviews that improved the paper. This work was supported by the Leverhulme Trust (RPG-2013-106).